JGR Biogeosciences

RESEARCH ARTICLE
10.1029/2019JG005569

This article is a companion to Kranz et al. (2020), https://doi.org/10.1029/2019JC015984

# Lagrangian Studies of Net Community Production: The Effect of Diel and Multiday Nonsteady State Factors and Vertical Fluxes on $O_2$/Ar in a Dynamic Upwelling Region

**Seaver Wang[1], Sven A. Kranz[2], Thomas B. Kelly[2], Hajoon Song[3], Michael R. Stukel[2], and Nicolas Cassar[1]**

[1]Nicholas School of the Environment, Division of Earth and Ocean Sciences, Duke University, Durham, NC, USA, [2]Department of Earth, Ocean and Atmospheric Sciences, Florida State University, Tallahassee, FL, USA, [3]Department of Atmospheric Sciences, Yonsei University, Seoul, South Korea

**Abstract** The ratio of dissolved oxygen to argon in seawater is frequently employed to estimate rates of net community production (NCP) in the oceanic mixed layer. The in situ $O_2$/Ar-based method accounts for many physical factors that influence oxygen concentrations, permitting isolation of the biological oxygen signal produced by the balance of photosynthesis and respiration. However, this technique traditionally relies upon several assumptions when calculating the mixed-layer $O_2$/Ar budget, most notably the absence of vertical fluxes of $O_2$/Ar and the principle that the air-sea gas exchange of biological oxygen closely approximates net productivity rates. Employing a Lagrangian study design and leveraging data outputs from a regional physical oceanographic model, we conducted in situ measurements of $O_2$/Ar in the California Current Ecosystem in spring 2016 and summer 2017 to evaluate these assumptions within a "worst-case" field environment. Quantifying vertical fluxes, incorporating nonsteady state changes in $O_2$/Ar, and comparing NCP estimates evaluated over several day versus longer timescales, we find differences in NCP metrics calculated over different time intervals to be considerable, also observing significant potential effects from vertical fluxes, particularly advection. Additionally, we observe strong diel variability in $O_2$/Ar and NCP rates at multiple stations. Our results reemphasize the importance of accounting for vertical fluxes when interpreting $O_2$/Ar-derived NCP data and the potentially large effect of nonsteady state conditions on NCP evaluated over shorter timescales. In addition, diel cycles in surface $O_2$/Ar can also bias interpretation of NCP data based on local productivity and the time of day when measurements were made.

**Plain Language Summary** Marine microbes produce and consume oxygen as a product of a balance between photosynthesis and respiration, thereby causing changes in the concentration of oxygen in the surface ocean. Taking advantage of known relationships between the gas properties of oxygen and argon, researchers can isolate changes in biologically produced oxygen from changes that result from physical processes. This calculation relies on several simplifying assumptions. In this study, we test the importance of these assumptions by tracking changes in biological oxygen while following several water parcels over the course of 2–4 days. We find that accounting for vertical mixing processes and the rate of change in biological oxygen is important when estimating biological oxygen production rates. We also find that daily shifts in oxygen as photosynthesis rises through the day and falls to zero at night can influence measurements based on time of collection.

**Key Points:**
- We employ Lagrangian observations of $O_2$/Ar in the California Current to test assumptions inherent to the $O_2$/Ar-based NCP method
- We demonstrate the significance of vertical fluxes and diel patterns in $O_2$/Ar that can bias NCP measurements
- Nonsteady state conditions and vertical fluxes strongly complicate efforts to evaluate $O_2$/Ar-based NCP on short timescales

**Supporting Information:**
- Supporting Information S1

**Correspondence to:**
S. Wang,
seaverwa@gmail.com

**Citation:**
Wang, S., Kranz, S. A., Kelly, T. B., Song, H., Stukel, M. R., & Cassar, N. (2020). Lagrangian studies of net community production: The effect of diel and multiday nonsteady state factors and vertical fluxes on $O_2$/Ar in a dynamic upwelling region. *Journal of Geophysical Research: Biogeosciences*, *125*, e2019JG005569. https://doi.org/10.1029/2019JG005569

Received 15 NOV 2019
Accepted 6 MAR 2020
Accepted article online 16 APR 2020

**Author Contributions:**
**Conceptualization:** Sven A. Kranz, Thomas B. Kelly, Michael R. Stukel, Nicolas Cassar
**Data curation:** Sven A. Kranz, Thomas B. Kelly, Hajoon Song
**Formal analysis:** Sven A. Kranz, Thomas B. Kelly
**Investigation:** Sven A. Kranz, Thomas B. Kelly, Michael R. Stukel, Nicolas Cassar
**Methodology:** Sven A. Kranz, Thomas B. Kelly, Hajoon Song, Michael R. Stukel, Nicolas Cassar
*(continued)*



## 1. Introduction

Basic measurements of oceanic primary production are essential to studying marine carbon fluxes, ecosystem dynamics, and carbon biogeochemistry. Marine net primary production, which accounts for half of total global primary production (Field et al., 1998), plays a correspondingly important role in regulating carbon fluxes between the atmosphere and the biosphere. Furthermore, marine biological uptake of inorganic carbon represents a key global climate feedback, with sequestration of sinking organic biomass into the deep ocean acting as a sink for atmospheric carbon. Improving the accuracy of marine primary production measurements can enhance our ability to both constrain the potential strength of this carbon pump to the ocean interior as well as to study marine ecosystems.

**Resources:** Sven A. Kranz, Michael R. Stukel, Nicolas Cassar
**Software:** Thomas B. Kelly, Hajoon Song
**Supervision:** Sven A. Kranz, Michael R. Stukel, Nicolas Cassar
**Validation:** Thomas B. Kelly, Hajoon Song
**Visualization:** Thomas B. Kelly, Michael R. Stukel
**Writing - original draft:** Sven A. Kranz, Thomas B. Kelly, Hajoon Song
**Writing – review & editing:** Sven A. Kranz, Hajoon Song, Michael R. Stukel, Nicolas Cassar

Numerous approaches for measuring marine primary production exist, spanning multiple incubation-based and in situ methods (Chavez et al., 2010; Ducklow & Doney, 2013). Within the last decade, an increasing number of studies (e.g., Cassar et al., 2011; Eveleth et al., 2017; Stanley et al., 2010; Ulfsbo et al., 2014; Wang et al., 2018) are utilizing underway techniques to continuously measure tracers of productivity in the surface ocean at fine resolution. Currently, an underway method in prevalent use employs measurements of the dissolved $O_2$/Ar ratio in seawater using either Equilibrator Inlet Mass Spectrometry (EIMS) (Cassar et al., 2009) or Membrane Inlet Mass Spectrometry (MIMS) (Kaiser et al., 2005; Tortell, 2005).

The $O_2$/Ar method is based upon isolation of the biologically driven signal in dissolved oxygen saturation within the surface ocean mixed layer and is widely used to generate estimates of surface net community production (NCP), defined as the difference between gross primary production and community respiration. NCP represents the net production of biomass remaining after accounting for consumption of organic carbon via respiration and thus reflects the total biological production available for export to depth (Berger & Wefer, 1990; Ducklow & Doney, 2013; Dugdale & Goering, 1967; Li & Cassar, 2017; Williams et al., 1989). While dissolved oxygen concentrations alone are subject to physical influences (temperature, atmospheric pressure, and bubble injection) in addition to biological drivers (photosynthesis and respiration), dissolved argon is not utilized in biological processes and possesses similar physical and temperature-based solubility characteristics compared to oxygen (Craig & Hayward, 1987). Consequently, changes in the ratio of dissolved $O_2$/Ar reflect biological production/respiration over the residence time of oxygen within the surface mixed layer. By measuring the $O_2$/Ar ratio in surface seawater continuously, the EIMS and MIMS techniques enable the collection of large NCP data sets with unprecedented spatiotemporal resolution. These methods represent important recent methodological advances in marine biogeochemistry.

While powerful, the $O_2$/Ar method is subject to some limitations. The $O_2$/Ar tracer can be influenced by advection and mixing of neighboring or subsurface waters with contrasting $O_2$/Ar signatures into the volume being sampled. In addition, assumptions involved in the parameterization of the air-sea gas exchange term represent a significant source of uncertainty (Bender et al., 2011). Diel variations in the magnitude of the $O_2$/Ar-derived biological oxygen saturation anomaly have also been commonly observed across a range of ocean settings (Ferron et al., 2015; Hamme et al., 2012; Tortell et al., 2014). The signal from diel cycling in the biological oxygen saturation anomaly is superimposed over underway measurements of $O_2$/Ar, thereby influencing spatial surveys based on the time of day at which observations are recorded. Such diel oscillations in the biological oxygen saturation anomaly vary in amplitude, ranging from ~0.2% in the oligotrophic North Pacific Subtropical Gyre (Ferron et al., 2015) to up to ~2% or more during highly productive blooms off the Antarctic coast (Tortell et al., 2014).

The in situ $O_2$/Ar method was traditionally a steady-state approach, in which mixed-layer biological oxygen production is balanced by efflux to the atmosphere over the residence time of oxygen in the surface mixed layer (Reuer et al., 2007). Both field (Hamme et al., 2012; Tortell et al., 2014) and model-based (Jonsson et al., 2013; Tortell et al., 2014) studies have indicated that steady-state conditions can be violated in practice over both diel and multiday timescales, particularly during periods of intense or rapidly changing biological production and/or when measurements capture physical effects such as entrainment due to changes in mixed-layer depth (MLD). However, a recent analysis (Teeter et al., 2018) concludes that the steady state assumption is not strictly required to estimate NCP on timescales several times longer than the surface residence time of biological oxygen, as the gas flux rate closely matches an exponentially weighted time average of past NCP rates even if nonsteady state conditions are present. Over shorter timescales however, ocean-atmosphere biological oxygen flux can significantly diverge from NCP rates under nonsteady state conditions, causing issues when attempting to interpret $O_2$/Ar-based NCP on shorter time scales, such as when making intermethod comparisons with in situ productivity rates.

In recent years, investigators have made efforts to better address and to correct for the abovementioned sources of error. The contribution of vertical fluxes of $O_2$/Ar to the mixed-layer biological oxygen balance has now been estimated in field studies using a variety of approaches ranging from oxygen profile-based calculations of entrainment and vertical eddy diffusive fluxes (Castro-Morales et al., 2013; Haskell et al., 2016) to quantification of the total vertical mixing flux using an $N_2O$-based approach (Cassar & Manizza, 2014; Izett et al., 2018). Furthermore, continued efforts have been made to examine the influence of nonsteady

state factors and to further improve the accuracy of the gas exchange parameterization term (Teeter et al., 2018). While non-Lagrangian study designs necessarily increase the difficulty of estimating the impact of diel and multiday nonsteady state changes in the biological oxygen saturation anomaly, efforts have also been made to quantify these factors in Lagrangian (Hamme et al., 2012) and stationary (Tortell et al., 2014) field settings.

The California Current upwelling zone is a highly dynamic coastal ecosystem characterized by steep cross-shore gradients in physical and biochemical conditions (Lynn & Simpson, 1987). Strong coastal upwelling in this region is driven by wind circulation, which generates sustained upwelling and Ekman transport along much of the California coastline (Chelton, 1982; Ohman et al., 2013; Rykaczewski & Checkley, 2008). Rising waters from depth carry high nutrient concentrations, fueling dramatic ecosystem production rates throughout much of the growing season (Munro et al., 2013; Ohman et al., 2013). With nitrogen and phosphorus in ample supply, portions of this region have been demonstrated to exhibit iron limitation (Hutchins et al., 1998; King & Barbeau, 2007). Productivity in the California Current Ecosystem (CCE) often follows a seasonal cycle, with the peak of the spring bloom typically occurring in April–May, followed by continued high production into the summer prior to subsiding over the course of the fall to low winter productivity rates (Munro et al., 2013). Offshore and alongshore currents, influenced by both Ekman transport and mesoscale and submesoscale fronts and eddies also lead to substantial mesoscale spatial variability and large advective fluxes (Landry et al., 2012; Strub & James, 2000).

Given its strong vertical and lateral fluxes, considerable spatial variability, and high rates of productivity, the California Current region arguably represents a "worst-case" field environment for the assumptions made when measuring NCP using traditional underway measurements of $O_2$/Ar. Errors associated with such conditions are often considerable, leading investigators to discard data collected within regions influenced by strong upwelling or to avoid field deployments in such regions altogether (Cassar & Manizza, 2014; Reuer et al., 2007). Because of this practice, however, only relatively few attempts (Haskell & Fleming, 2018) have been made to quantify the sources of error within such a challenging setting to date. Such efforts have the potential to help us more critically evaluate the strengths and weaknesses of the assumptions involved in calculating community production rates from dissolved $O_2$/Ar.

In this paper, we present Lagrangian in situ measurements of $O_2$/Ar saturation anomalies and NCP from seven multiday deployments over two field expeditions in the CCE in spring 2016 and 2017. This dynamic region represents a unique study environment for assessing the respective impact of diel and multiday nonsteady state conditions and vertical fluxes upon $O_2$/Ar-derived estimates of NCP on short-term (multiday) and longer-term (30-day exponentially weighted) timescales. By estimating the contribution over time of vertical $O_2$/Ar fluxes as well as diel and longer-term nonsteady state conditions to the overall biological oxygen signal in various water masses within this region, we demonstrate the critical importance of accounting for such potential sources of measurement error, underlining the need for quantification of these factors via concurrent $N_2O$ sampling and/or other means when measuring NCP in similarly dynamic ocean regions around the world.

## 2. Methods

### 2.1. Cruise Background

Underway measurements and conductivity-temperature-depth (CTD)-Niskin rosette casts were conducted during an expedition aboard the *R/V Sikuliaq* from 19 April to 12 May 2016 during the RAPID CCE-LTER process cruise (P1604), as well as from 1 June to 2 July 2017 aboard the *R/V Roger Revelle* during the subsequent year's CCE-LTER process cruise (P1706) (Figure 1). Three to four quasi-Lagrangian experiments (hereafter "cycles") were conducted in each year while following selected water masses over ~3-day periods at various locations in the CCE. Following the completion of a towed Moving Vessel Profiler survey of the local area to ensure that the deployment site represented a cohesive water mass free of strong frontal gradients (Landry et al., 2012; Ohman et al., 2012; Stukel et al., 2013), each cycle began when a drogued sediment trap array and a drogued experimental array were deployed (Landry et al., 2009; Stukel et al., 2013). Each array included a 3 × 1-m holey sock drogue centered at 15-m depth to track the mixed layer (10–81 m) (Landry et al., 2009; Niiler et al., 1995).

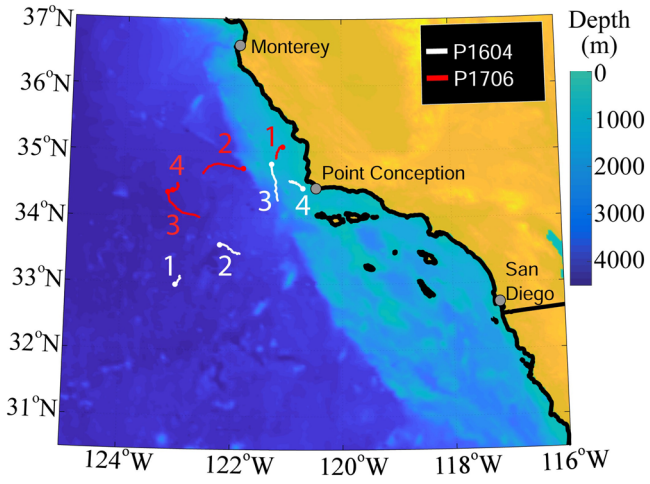


**Figure 1.** Map of cruise tracks during Lagrangian deployments in spring 2016 and summer 2017 within the California Current Ecosystem. White lines indicate observations in 2016. Red lines denote cycle locations in 2017. Colored dots mark the starting location for each cycle. Numbering indicates chronological order of cycles in 2016 and 2017. Background blue color scale indicates regional bathymetry.

In 2016, the first Lagrangian cycle (P1604-1) was aborted due to an on-ship emergency and we do not evaluate data collected during this deployment. The second cycle (P1604-2) was located within the heart of the California Current, while the third and fourth cycles were both situated within the inshore zone of sustained upwelling off Point Conception (Table 1). P1604-3 was located within the wind stress curl upwelling region, while P1604-4 was conducted inside the coastal boundary upwelling zone. For additional details on plankton communities during the P1604 cruise, see Morrow et al. (2018) and Nickels and Ohman (2018). During the 2017 cruise, the first cycle was conducted in the inshore upwelling region, the second cycle was initiated in aged upwelled waters and lasted 4 days, and the third cycle was conducted in postbloom waters. The fourth cycle in 2017 (P1706-4) lasted 2 days and represented a "continuation" of P1706-2 where the *Revelle* returned to a surface-tethered drifting sediment trap, which had been deployed at the end of P1706-2. All other deployments in 2016 and 2017 apart from P1706-2 and P1706-4 were conducted for a duration of 3 days.

### 2.2. Underway $O_2$/Ar Measurements via EIMS

Using the EIMS method (Cassar et al., 2009), we conducted high-resolution measurements of the dissolved $O_2$/Ar ratio in surface seawater. Briefly, intake seawater collected at a depth of 5 m by the ship's underway system was circulated continuously via a magnetic gear pump through a membrane contactor. Within the membrane contactor, dissolved gases from the seawater flow rapidly equilibrate within the headspace at pressures reflecting in situ concentrations. Equilibrated gas was measured using a Pfeiffer Prisma QMS 200 M1 quadrupole mass spectrometer. Every 2–4 hr, an automated program or user input was used to switch a multiport Valco valve in order to sample ambient room air from a second capillary of equal length for 20–30 min. These "air calibrations," measuring the constant ratio of atmospheric $O_2$/Ar, are used in downstream processing to express the in situ $O_2$/Ar saturation anomaly relative to the ratio at atmospheric equilibrium and to calibrate "water" $O_2$/Ar measurements for instrumental drift.

Apart from occasional breaks in measurements for cleaning, service, or to troubleshoot technical issues, EIMS measurements were collected continuously throughout both cruises during all Lagrangian cycles. Gaps in data due to instrument downtime never exceeded 4.5 hr during Lagrangian measurements, apart from a 9.5-hr break in data during the first cycle of P1706.

Potential respiration in the ship's lines (Juranek et al., 2010) was assessed in 2016 using five paired sets of discrete Winkler dissolved oxygen samples taken from CTD casts and from the underway seawater tap over the course of the cruise. Winkler samples from CTD casts were collected from a surface depth of around five meters. Samples were immediately fixed with pickling reagents and measured via Winkler titration at Scripps Institute of Oceanography shortly after returning to port following the procedure outlined in the CalCOFI program's Winkler sampling and analysis protocol (http://www.calcofi.org/ccpublications/calcofi-methods/13-dissolved-oxygen.html). Measured Winkler samples showed no consistent difference between underway and in situ oxygen concentrations (average offset of $<0.43$ μmol kg$^{-1}$, standard deviation of 1.73 μmol kg$^{-1}$, average percent difference of −0.1%), suggesting that the effect of microbial respiration in the *R/V Sikuliaq's* underway plumbing was negligible. In situ Winkler samples were not taken during the P1706 cruise.

### 2.3. Calculation of Biological Oxygen Saturation Anomaly ($\Delta O_2$/Ar)

Raw EIMS data were time averaged at a 2-min time step. Mass spectrometer data collected during testing, periods of technical failure, and during shutoffs of the ship's underway seawater flow were filtered using times recorded in a cruise log sheet. EIMS data collected during periods in which mass spectrometer pressure were anomalously high or low ($<1 \times 10^{-6}$ or $>9 \times 10^{-6}$ mbar), as well as data recorded during the 80-min period following any instrument restart were also filtered. At times when a valve switch between

**Table 1**
*Basic Metadata for Lagrangian Observations Conducted in 2016 and 2017*

| Cycle | Latitude (N) | Longitude (E) | Date/time (PST) | $O_2$ residence time (day) | Temperature (°C) | MLD (m) | Chl-*a* ($\mu g\ L^{-1}$) |
|---|---|---|---|---|---|---|---|
| P1604–2 | 33.59 | −122.22 | 28 Apr 2016 21:07 | 16.2 (1.2) | 15.4 (0.1) | 70 (4) | 0.1 (0.0) |
| P1604–3 | 34.77 | −121.29 | 2 May 2016 23:47 | 6.8 (0.7) | 14.0 (0.3) | 17 (0) | 1.1 (0.2) |
| P1604–4 | 34.50 | −120.79 | 7 May 2016 21:23 | 9.8 (0.4) | 14.8 (0.3) | 14 (1) | 4.1 (0.8) |
| P1706–1 | 35.07 | −121.09 | 9 Jun 2017 01:29 | 9.0 (1.0) | 13.3 (0.3) | 20 (6) | 9.3 (2.7) |
| P1706–2 | 34.73 | −121.71 | 13 Jun 2017 02:55 | 4.4 (0.7) | 13.2 (0.2) | 27 (1) | 3.1 (1.0) |
| P1706–3 | 34.38 | −123.17 | 18 Jun 2017 01:46 | 2.9 (0.8) | 15.2 (0.6) | 18 (4) | 0.6 (0.5) |
| P1706–4 | 34.40 | −123.07 | 23 Jun 2017 01:50 | 4.7 (0.6) | 15.7 (0.5) | 12 (0) | 0.2 (0.1) |

*Note*. Lat/Lon coordinates, date, and time are given as the starting values for each cycle. Parameters are listed as mean cycle values, with values in parentheses indicating standard deviations.

air and water capillaries occurred, the nearest 6 min of water measurements and the nearest 4 min of air measurements were also filtered from the data set to avoid transition artifacts.

Biological $O_2$ saturation anomaly was subsequently calculated from the measured ion current ratio according to the following formula:

$$Biological\ O_2\ sat\ anomaly = \Delta(O_2/Ar) = \left(\frac{(O_2/Ar)_{measured}}{(O_2/Ar)_{saturation}} - 1\right) \quad (1)$$

where $O_2/Ar_{measured}$ corresponds to the oxygen-argon ratio measured from sampled seawater and $O_2/Ar_{saturation}$ represents the $O_2$/Ar ratio expected at air-sea gas exchange equilibrium, which is assumed to correspond to the $O_2$/Ar ratio found in air. A continuous vector of $O_2/Ar_{equil}$ values was generated by calculating the mean $O_2$/Ar recorded during each air calibration, followed by linear interpolation of the $O_2/Ar_{equil}$ ratio between each set of successive air calibrations. Data collected between air calibrations at which the difference in $O_2$/Ar exceeded 0.02 were filtered, as were data collected when the interpolated ion current ratio of air measurements was outside the range of 15 to 28. Following filtration of anomalous data, the $\Delta O_2$/Ar data set was then merged with 2-min-averaged ship data (time, position, temperature, salinity, photosynthetically active radiation, and wind speed).

MLD calculations, subsurface oxygen concentrations, and oxycline gradients are necessary for parameterizing the gas exchange term for NCP calculations and to estimate vertical $O_2$/Ar fluxes from vertical entrainment, eddy diffusion, and advective fluxes. These parameters were calculated from CTD cast measurements conducted during both the 2016 and 2017 cruises. Quality-checked, 1-m depth-averaged CTD cast data was downloaded from the CCE LTER online database (https://oceaninformatics.ucsd.edu/datazoo/catalogs/ccelter/datasets). MLDs were determined using a density difference criterion of 0.03 kg $m^{-3}$ from the density measurement at a reference depth of 10 m (Dong et al., 2008). Additionally, using bisector least squares regression, oxygen measurements from the 20 m below the calculated MLD were used to determine subsurface gradients in oxygen immediately below the mixed layer. MLD values and oxygen gradients were then linearly approximated across each cycle.

As the residence time of $\Delta O_2$/Ar in the surface ocean is on the order of days to weeks, prior local wind speed data from the period preceding real-time measurements are required to incorporate wind speed history into parameterization of the gas transfer velocity. Daily North American Regional Reanalysis (NARR) wind speeds in the 30-day period prior to the day of measurement were downloaded from the National Oceanic and Atmospheric Administration Earth System Research Laboratory online database (https://www.esrl.noaa.gov/psd/data/gridded/data.narr.monolevel.html) then 2-D interpolated to yield wind speed history data along our cruise coordinates. For both years of NARR data, we compared NARR and 10-m height-corrected (Thomas et al., 2005) ship-measured wind speeds then corrected the former using a linear model to more closely match field wind speed data. Ship and uncorrected NARR wind speeds tracked changes in wind speeds over time similarly, although NARR wind speed data typically exceeded ship-recorded winds. We observed a mean offset of 2.1 m $s^{-1}$ (std dev: 2.2 m $s^{-1}$). Gas transfer velocity was parameterized following (Wanninkhof, 2014), applying the wind speed history-based weighting scheme of (Reuer et al., 2007) with the modification advocated by (Teeter et al., 2018).

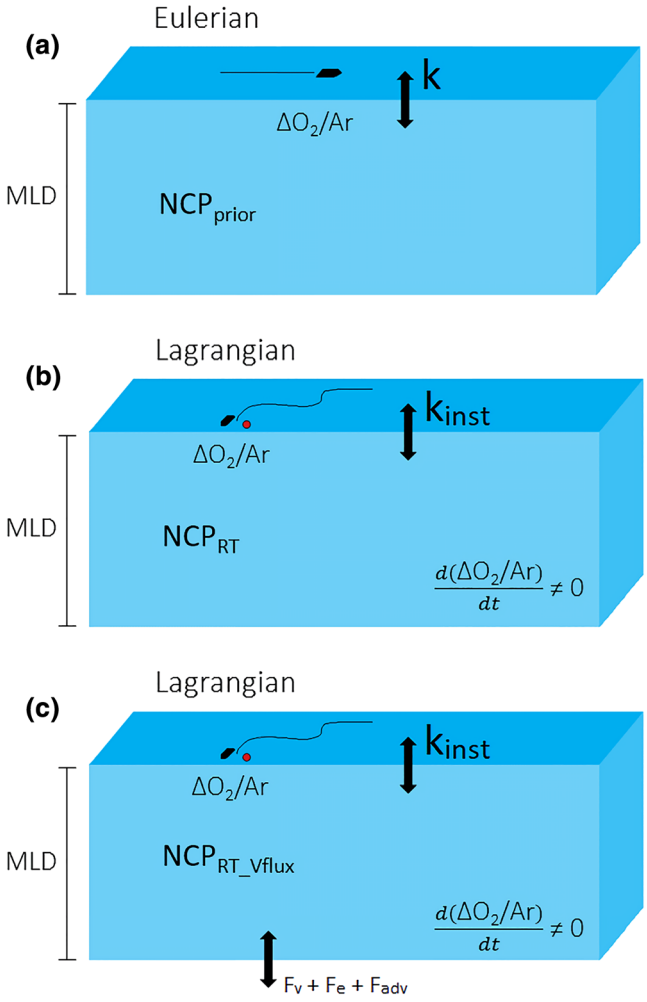


**Figure 2.** Conceptual diagram illustrating underlying assumptions behind three models for $O_2$/Ar-derived NCP: $NCP_{prior}$, $NCP_{RT}$, and $NCP_{RT\_Vflux}$.

Exponentially weighted NCP rates, reflecting raw biological oxygen fluxes uncorrected for vertical mixing, were calculated using equation 2:

$$NCP_{prior}\left(\text{mmol O}_2\ \text{m}^{-2}\ \text{day}^{-1}\right) = \Delta O_2/Ar \cdot [O_2]_{sol} \cdot \rho \cdot k \quad (2)$$

where $\Delta O_2/Ar$ signifies the $O_2$/Ar saturation anomaly relative to atmospheric equilibrium (see equation 1), $\rho$ represents the density of seawater (kg $m^{-3}$) as calculated from the UNESCO 1983 equation of state, and $k$ denotes the weighted gas transfer velocity. Lastly, $[O_2]_{sol}$ is the oxygen concentration at saturation, calculated from (Garcia & Gordon, 1992, 1993).

Following calculation of preliminary NCP data, a distance filter was applied to remove likely non-Lagrangian data collected at distances of more than 8 km from the sediment trap and drifter array. We further calculated uncertainty associated with $NCP_{prior}$ values (not including vertical fluxes), by propagating uncertainty in the following terms: $k$ (20%; Wanninkhof, 2014), $\Delta O_2/Ar$ (0.3%; Cassar et al., 2009).

These uncorrected NCP data represent an exponentially weighted average of NCP over the residence time of oxygen within the mixed layer, so we henceforth term this calculated rate as $NCP_{prior}$ as in (Hamme et al., 2012). An open source pipeline of R scripts has been developed to perform $NCP_{prior}$ calculations and was used to process data from both cruises (Kelly, 2019).

### 2.4. Detrending and Curve Fitting of $NCP_{prior}$ Data and Calculation of Diel Cycle Characteristics

To better isolate and quantify the diel pattern of $\Delta O_2/Ar$ and measured $NCP_{prior}$ observed at each cycle, our raw data required detrending to remove the long-term nondiel rate of change. We further matched a fitted curve to each cycle's data to model the observed diel pattern in the data.

Linear models (using the "regstats" function in MATLAB) were fit to a subset of each cycle's data beginning and ending at the same time of day (typically around 4 a.m. local time). Linear trends were observed for all cycles apart from P1604-2, although the observed slopes were modest for several of the cycles. For each cycle, the trend line was subtracted from the data in order to detrend the cycle $NCP_{prior}$ for greater ease of isolating the diel signal. All regressions were statistically significant ($p \ll 0.01$).

To model the observed diel cycle of $NCP_{prior}$ rates for each Lagrangian study, a Fourier series was fit to the corrected, detrended $NCP_{prior}$ data using the curve fitting toolbox in MATLAB. In most cases, we selected the most parsimonious Fourier series fit that gave the correct number of diel cycles for the observation period. This generally corresponded to a four-term Fourier series fit apart from P1706-4, where we employed a three-term fit due to the abbreviated length (two days) of this cycle. For P1604-3 and P1706-2, a fifth term was added to further improve the goodness of fit.

Local times for apparent sunrise and sunset were calculated using the National Oceanic and Atmospheric Administration Earth System Research Laboratory Solar Calculator (https://www.esrl.noaa.gov/gmd/grad/solcalc/), using the cycle dates and starting coordinates of each Lagrangian cycle as inputs.

The approximate range of the diel variability in $\Delta(O_2/Ar)$ and $NCP_{prior}$ rates was calculated from the median of the daily maxima and minima of raw $\Delta(O_2/Ar)$ and $NCP_{prior}$ values observed over the course of a particular multiday cycle.

### 2.5. Assessment of Nonsteady State Impacts on Calculated NCP

Due to our Lagrangian study design, we were able to measure the change in mixed-layer $\Delta O_2/Ar$ in real time over the observational period and thereby theoretically estimate NCP over a shorter timescale without

having to employ an assumption of steady state (Figure 2). To do this, we utilized equation 2 of Hamme et al. (2012):

$$NCP_{RT} = k_{inst}(\Delta O_2/Ar)[O_2]_{sol}\rho + z\frac{d(\Delta O_2/Ar)}{dt}[O_2]_{sol}\rho \quad (3)$$

Note that $k_{inst}$ represents the unweighted rather than weighted gas exchange coefficient, using daily averaged wind on the day of observations. $z$ denotes the MLD.

Similar to when detrending uncorrected $NCP_{prior}$ data as described above, the long-term (over the period of observation) rate of change in $\Delta(O_2/Ar)$ (i.e., $\frac{d(\Delta O_2/Ar)}{dt}$ in equation 3) was determined via a linear regression, yielding the slope of $\Delta(O_2/Ar)$ measurements for each cycle. To minimize the influence of diel changes in $\Delta(O_2/Ar)$ upon the calculated multiday slope, each cycle's data were trimmed to start and end at the same time of day as previously described. All relationships obtained for $\Delta(O_2/Ar)$ linear regressions were statistically significant ($p \ll 0.01$).

Following the terminology of (Hamme et al., 2012), we henceforth refer to our NCP rates calculated using the above method, evaluated over a multiday timescale without the use of a steady-state assumption, as real-time NCP ($NCP_{RT}$). We further calculated uncertainty associated with $NCP_{RT}$ values (not including vertical fluxes), by propagating uncertainty in the following terms: $k_{inst}$ (20%; Wanninkhof, 2014), $\Delta O_2/Ar$ (0.3%; Cassar et al., 2009), $z$ (5 m; Hamme et al., 2012), and $\frac{d(\Delta O_2/Ar)}{dt}$ (using the standard error of the linear model).

### 2.6. Calculation of Vertical $O_2$/Ar Fluxes

Following Castro-Morales et al. (2013) and Emerson et al. (2008), the vertical flux-corrected mass balance of biological oxygen in the surface ocean would be expressed as follows:

$$NCP_{Vflux} = NCP_{prior} + F_v + F_e + F_{adv} \quad (4)$$

where $F_v$ and $F_e$ represent the impact of vertical eddy diffusive flux and entrainment flux, respectively, $F_{adv}$ denotes the advective flux, and $NCP_{prior}$ represents the uncorrected NCP (see equation 2). We estimated the magnitude of vertical eddy diffusion and entrainment fluxes to mixed-layer biological oxygen fluxes following (Castro-Morales et al., 2013)

$$F_v = -K_z \cdot \frac{\partial[O_2]}{\partial z}_{oxycline} \quad (5)$$

$$F_e = -\frac{1}{2}\frac{(\Delta z_{mix})^2}{\Delta t} \cdot \frac{\partial[O_2]}{\partial z}_{oxycline} \quad (6)$$

where $K_z$ represents the eddy diffusivity coefficient ($m^2\ s^{-1}$), $\frac{\partial[O_2]}{\partial z}_{oxycline}$ the gradient of oxygen in the 20 m beneath the MLD, and $\Delta z_{mix}$ the change in MLD over the time interval between CTD casts ($\Delta t$). Negative values for $F_v$ and $F_e$ in equations 5 and 6 represent vertical addition of biological $O_2$ to the mixed layer resulting from increasing oxygen with depth, while decreasing oxygen with depth results in positive values for $F_v$ and $F_e$.

Advective flux of biological oxygen into the mixed layer from the subsurface was calculated using the following equation:

$$F_{adv} = -w \cdot \frac{\partial[O_2]}{\partial z}_{oxycline} \cdot z_{mix} \quad (7)$$

where $w$ denotes the vertical velocity (positive upward) and $z_{mix}$ represents the MLD. Upward vertical velocities (positive) and increasing oxygen with depth thus result in negative $F_{adv}$, and vice versa. Note that advective fluxes are only significant in the case of upwelling—in the absence of large horizontal gradients in $O_2$/Ar, downwelling does not alter the biological $O_2$ concentration of the mixed layer, and so we assume that $F_{adv} = 0$ when $w < 0$.

Values for $K_z$ and $w$ were extracted from a three-dimensional physical model (9-km horizontal resolution, 42 vertical layers) developed using the Regional Ocean Modeling System (ROMS) four-dimensional variational data assimilation system (4DVAR) (Moore et al., 2011), then depth-interpolated linearly to calculate values at the MLD. Initial and boundary conditions were taken from the California Current System Reanalysis product produced by the University of California, Santa Cruz. Surface forcing was taken from the 9-km-resolution Coupled Ocean/Atmosphere Mesoscale Prediction System (Doyle et al., 2009; Hodur, 1997). We assimilated satellite remote sensing products, including sea surface height from Ssalto/Duacs (59964 observations) and sea surface temperature from the Advanced Very High Resolution Radiometer (357,063 observations), surface current data from coastal high-frequency radar observations (39,127 observations), and in situ temperature and salinity data vertical profiles collected during CTD measurements on our cruise (30,675 observations). Assimilated data were used to update model initial conditions and surface forcing to generate a dynamically consistent monthlong model fit covering the duration of each cruise and producing 8-hr-averaged outputs. Following iterative updating of the incremental model, we obtained a reduction of the cost function, a metric reflecting the change in the model from its initial conditions as well as its success in minimizing differences between the model state and the observational data set, of 72% and 57% for the 2017 and 2016 model fits, respectively (Figure S1 in the supporting information). Reductions in the errors between observations and modeled values for surface currents, temperature, salinity, and sea surface height ranged between 24% and 74% (Table S1). For detailed descriptions of our ROMS 4DVAR approach, see Song et al. (2012) and Miller et al. (2015). $K_z$ and $w$ were interpolated to CTD cast locations from the 9-km ROMS 4DVAR solution using bilinear 2-D interpolation from the four points comprising the nearest neighbors to the cast coordinates. Median $K_z$ values and median positive vertical velocities ($w$) at the MLD for each Lagrangian cycle were then calculated and employed for vertical eddy diffusion and vertical advection estimates.

Incorporating these vertical flux estimates into our calculation of $NCP_{RT}$ described above yields

$$NCP_{RT\text{-}Vflux} = k_{inst}(\Delta O_2/Ar)[O_2]_{sol}\rho + z\frac{d(\Delta O_2/Ar)}{dt}[O_2]_{sol}\rho + F_v + F_e + F_{adv} \quad (8)$$

$NCP_{RT\_Vflux}$ thereby captures both the multiday rate of change in the biological oxygen saturation anomaly over the observational period and the influence of vertical fluxes via eddy diffusion, entrainment, and advection.

Due to large uncertainties in $F_{adv}$ resulting from the use of modeled vertical velocities, we did not calculate $NCP_{RT\_VFlux}$ directly, as the margin of uncertainty associated with advective fluxes dwarfed the $O_2$/Ar signal. Potential error in the advective flux term was very large, to the point where $NCP_{RT\_VFlux}$ would no longer represent a meaningful estimate of community production. Instead, we separately calculated and report the magnitude and variability of the individual vertical flux components: $F_v$, $F_e$, and $F_{adv}$.

## 3. Results

### 3.1. General Patterns of NCP From Lagrangian Measurements in the California Current in Spring/Summer 2016 and 2017

In both 2016 and 2017, mean MLD-integrated $NCP_{prior}$ values observed during each cycle were largest at the cycles closest to the shore (Table 2 and Figure 3). The cycles conducted closest to shore exhibited mean $NCP_{prior}$ rates of 47 ± 11 and 68 ± 16 mmol $O_2$ $m^{-2}$ $day^{-1}$ for P1604-4 and P1706-1, respectively. Located just off the Point Conception upwelling center, these locations were distinguished by high Chl-*a* concentrations, peaks of $O_2$/Ar saturation anomaly (>15%) and large diel variation in the $O_2$/Ar signal (Figure 4). The range of $NCP_{prior}$ for a given cycle also broadened for cycles located closer to shore. Throughout the day, coastal $NCP_{prior}$ rates could exhibit a surprising degree of volatility, with rapid short-term changes in biological oxygen saturation anomaly of as much as 10% occurring at points during the observation period. Ecologically, we observed this coastal region to be a productive ecosystem rich in marine life. Algal biomass was high in the surface layer (~4 μg Chl-*a* $L^{-1}$), with high abundances of krill, copepods, and even tuna crabs (*Pleuroncodes planipes*) choking the *R/V Sikuliaq's* sea strainers during P1604-4. During the 2017 cruise the coastal region had high chlorophyll (surface Chl averaged 9 μg Chl-*a* $L^{-1}$) and high nutrient concentrations

**Table 2**
*Statistics for Community Production Rates, Vertical Flux Magnitudes, Oxygen Gradients, and Regression-Derived Slopes in $\Delta O_2/Ar$ and NCP for Each Cycle*

| Cycle | Mean $NCP_{prior}$ | Mean $NCP_{RT}$ | Range of $NCP_{RT}$ | Mean $F_v$ | Mean $F_e$ | Mean $F_{adv}$ | Range of $F_{adv}$ | $O_2$ gradient (mmol $O_2$ $m^{-4}$) | Slope in $\Delta O_2/Ar$ (% $day^{-1}$) | Slope in $NCP_{prior}$ (mmol $O_2$ $m^{-2}$ $day^{-2}$) |
|---|---|---|---|---|---|---|---|---|---|---|
| P1604–2 | 7 ± 5 (1) | −3 ± 7 (6) | −11 to 6 | 0 (1) | −1 (1) | −32 (108) | −302 to 153 | 0.1 (0.2) | −0.06 | −1 |
| P1604–3 | −2 ± 2 (13) | 84 ± 29 (4) | 73 to 91 | 1 (0) | 0 (0) | 44 (20) | 2 to 76 | −0.6 (0.2) | 1.95 | 13 |
| P1604–4 | 47 ± 11 (13) | −15 ± 35 (11) | −36 to 6 | 7 (0) | 2 (0) | 781 (556) | 60 to 2252 | −4.9 (0.3) | −1.00 | −4 |
| P1706–1 | 68 ± 16 (26) | −60 ± 85 (65) | −229 to 104 | 6 (1) | 96 (7) | 1085 (567) | 205 to 2580 | −4.2 (0.1) | −3.13 | 0 |
| P1706–2 | −22 ± 9 (24) | −72 ± 25 (33) | −128 to 66 | 22 (4) | 2 (0) | 745 (136) | 536 to 954 | −4.2 (0.5) | −0.63 | −13 |
| P1706–3 | −11 ± 7 (12) | −26 ± 12 (15) | −55 to 3 | 0 (0) | −1 (0) | −14 (9) | −32 to −4 | 0.1 (0.1) | −0.32 | −5 |
| P1706-4 | −1 ± 2 (4) | 14 ± 9 (1) | 10 to 16 | 1 (0) | 0 (0) | 48 (23) | −65 to −12 | −0.9 (0.3) | 0.45 | 3 |

*Note*. Values in parentheses indicate standard deviations. All units are in mmol $O_2$ $m^{-2}$ $day^{-1}$ unless otherwise stated. Positive values for $F_v$, $F_e$, or $F_{adv}$ indicate contributions of oxygen-undersaturated waters from below, while negative values denote upward introduction of supersaturated waters.

(surface $NO_3^-$ averaged 6 μmol $L^{-1}$). Data on the heterotrophic plankton community for the 2017 cruise were not yet available but will eventually be published on the CCE-LTER DataZoo database.

P1604-2, conducted in the heart of the California Current, was unique in several respects. For one, P1604-2 displayed a narrow range of low $NCP_{prior}$ rates (4 to 10 ± 1 mmol $O_2$ $m^{-2}$ $day^{-1}$) compared to all other cycles in both years (range for all other cycles was −66 to 127 mmol $O_2$ $m^{-2}$ $day^{-1}$. This location was also characterized by deeper MLDs (65 to 76 m) than all other cycles (10–30 m).

Cycles conducted further offshore (P1604-2, P1604-3, P1706-3, and P1706-4) shared similarities in terms of $NCP_{prior}$ rate ranges with values generally varying between −20 and 20 mmol $O_2$ $m^{-2}$ $day^{-1}$.

### 3.2. Exponentially Weighted Versus Short-Term, Nonsteady State-Based Calculation of In Situ NCP

Nonsteady state changes in mixed-layer biological oxygen implied by the slopes of the linear fits suggest that nonsteady state conditions were nonnegligible when integrated over multiple days, with changes in $\Delta O_2/Ar$

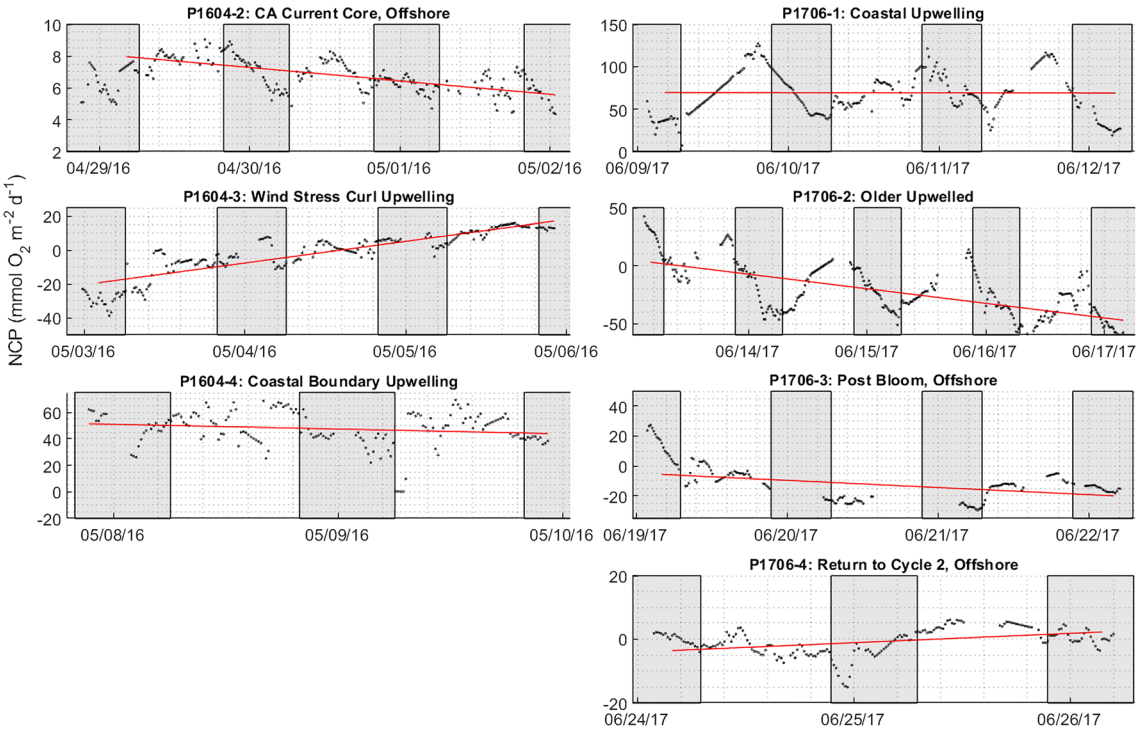


**Figure 3.** $NCP_{prior}$ measured for each Lagrangian cycle (black points). The line of best fit for each cycle's NCP data, derived from a linear regression against a subset of the cycle data beginning and ending at the same local time of day, is shown in red. Shaded sections of background indicate nighttime periods.

ranging from −3.13 to 1.95% saturation anomaly per day at some stations. The observed rates of change in the $NCP_{prior}$ signal across the cycles corresponded to slopes varying between −13 and 13 mmol $O_2$ $m^{-2}$ $day^{-2}$ (Table 2).

The secular increases and decreases in mixed-layer biological oxygen during a cycle resulted in corresponding offsets between $NCP_{RT}$ and $NCP_{prior}$ proportional to the magnitude of the slope in $\Delta O_2/Ar$. The relationship between $d$ $(\Delta O_2/Ar)/dt$ and the offset between $NCP_{RT}$ and $NCP_{prior}$ was statistically significant when tested using a linear model ($p < 0.001$, $R^2 = 0.97$, $n = 7$). These offsets were more modest (i.e., <15 mmol $O_2$ $m^{-2}$ $day^{-1}$ difference in median $NCP_{prior}$ versus $NCP_{RT}$) for stations located further offshore (P2016-2, P2017-3, and P2017-4) than for stations closer to the coast, where median real-time NCP over the measurement period differed from $NCP_{prior}$ by up to an order of magnitude and could even flip estimated NCP rates from positive to negative. For instance, $NCP_{RT}$ calculations for P1706-1 produce an overall strong negative biological oxygen flux, while $NCP_{prior}$ yields a strong positive flux (Table 2).

### 3.3. Diel Nonsteady State Variation in the $O_2$/Ar-Derived NCP Signal

Clear diel patterns were evident in both the measured $\Delta O_2/Ar$ saturation anomaly and calculated $NCP_{prior}$ rates across six of the seven sites occupied (Figure 5). Additionally, we observed a consistent pattern of increasing amplitude of the diel signal in $O_2/Ar$ with closer proximity to shore. Increasingly larger diel signal amplitudes also tended to correspond to stations at which more elevated Chl-*a* concentrations were also observed.

At the two stations closest to the coast, diel variations in biological oxygen saturation anomaly were dramatic, leading to approximately twofold changes in $\Delta O_2/Ar$ (%) over the course of a daylong period. The range of the diel signal at these inshore stations was also large: regularly over 10% and as large as 17%. Such oscillations are similar in magnitude to diel changes in $\Delta O_2/Ar$ (%) observed off the coast of Palmer Station on the West Antarctic Peninsula in summer (Tortell et al., 2014). This diel variability resulted in daily shifts of apparent measured $NCP_{prior}$ of up to ~100 mmol $O_2$ $m^{-2}$ $day^{-2}$ (Table 3). A greater degree of day-to-day variability in the magnitude of diel variation was also shown at inshore sites, with the amplitude of the diel pattern exhibiting changes of up to twofold throughout the observational period.

In contrast, the cycles furthest offshore also exhibited clear diel behavior, but with substantially smaller amplitude (changes in $\Delta O_2/Ar$ of <1 to 2% saturation anomaly). Nevertheless, such diel patterns are significant relative to the margin of error inherent to the method (~0.3%) and relative to the magnitude of the local NCP.

Two study locations, P1604-3 and P1706-3, did not demonstrate diel patterns with the same degree of clarity. This absence of a clear diurnal behavior for these cycles was related to strong multiday trends in the $\Delta O_2/Ar$ signal (Figure 3) possibly connected to an increase in wind speed during P1706-3.

### 3.4. Influence of Vertical Fluxes of $O_2$/Ar Upon Calculated In Situ NCP

Relative to the difference between $NCP_{prior}$ and $NCP_{RT}$, the influence of vertical $O_2/Ar$ fluxes was comparable and often even larger (Table 2). Consequently, the surface layer $O_2/Ar$ budget at our study locations is significantly and often dominantly influenced by the vertical flux terms.

Across all cycles, the influence of vertical advection dominated both other vertical fluxes, with advective fluxes an order of magnitude larger than $NCP_{prior}$ or $NCP_{RT}$ at some stations. Calculated ranges in vertical advective fluxes were generally large as well, in excess of 400 mmol $O_2$ $m^{-2}$ $day^{-1}$ at four of seven cycles with a maximum $F_{adv}$ rate of 2,580 mmol $O_2$ $m^{-2}$ $day^{-1}$ estimated for P1706-1. These values are, however, highly sensitive to the vertical velocity estimates used in calculations and to the strength of and variations in the subsurface $O_2$ gradient (i.e., −5.2 to −3.4 mmol $O_2$ $m^{-4}$ for P1706-2), which drive much of the variability in calculated advective fluxes.

Entrainment fluxes and vertical eddy diffusive fluxes were generally less influential than advective fluxes but could still represent nonnegligible sources of error. As entrainment flux only comes into effect upon a deepening of the surface mixed layer, cycle entrainment flux values were absent for some cycles during which MLDs predominantly shoaled or remained stable during the observed period. Both vertical eddy diffusion

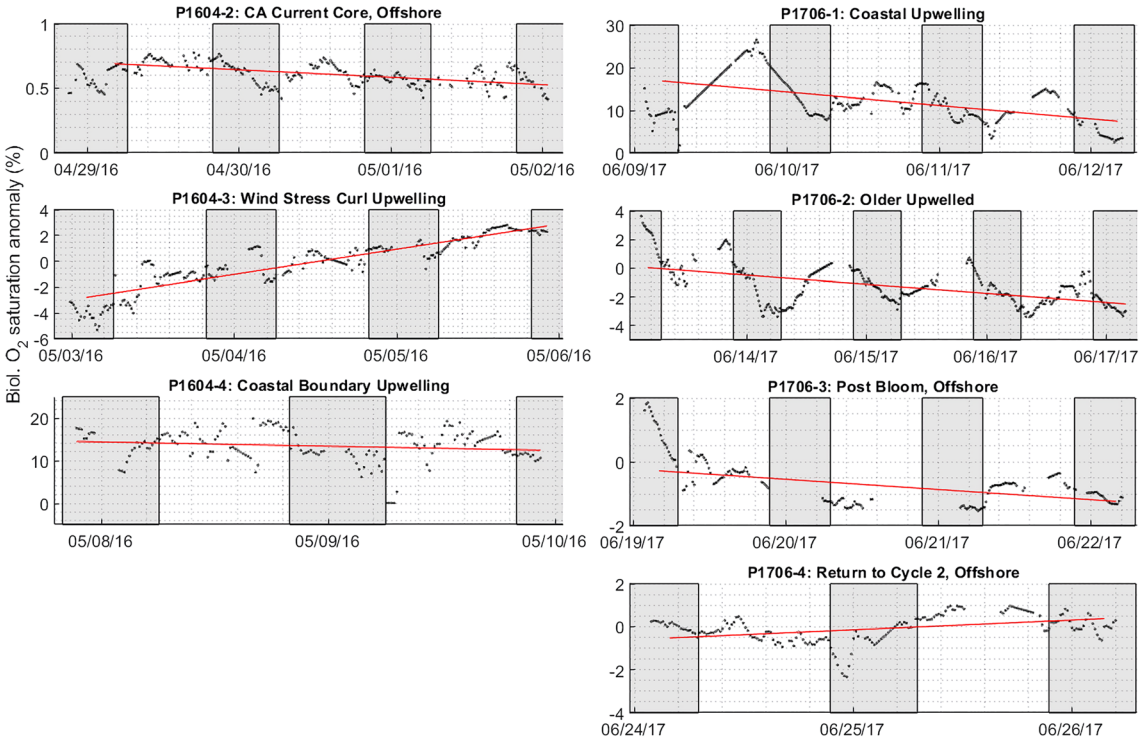


**Figure 4.** Time series of $\Delta O_2/Ar$ observations for each cycle (black). The line of best fit for each cycle's $\Delta O_2/Ar$ data, derived from a linear regression against a subset of the cycle data beginning and ending at the same local time of day, is shown in red. Shaded sections of background indicate nighttime periods.

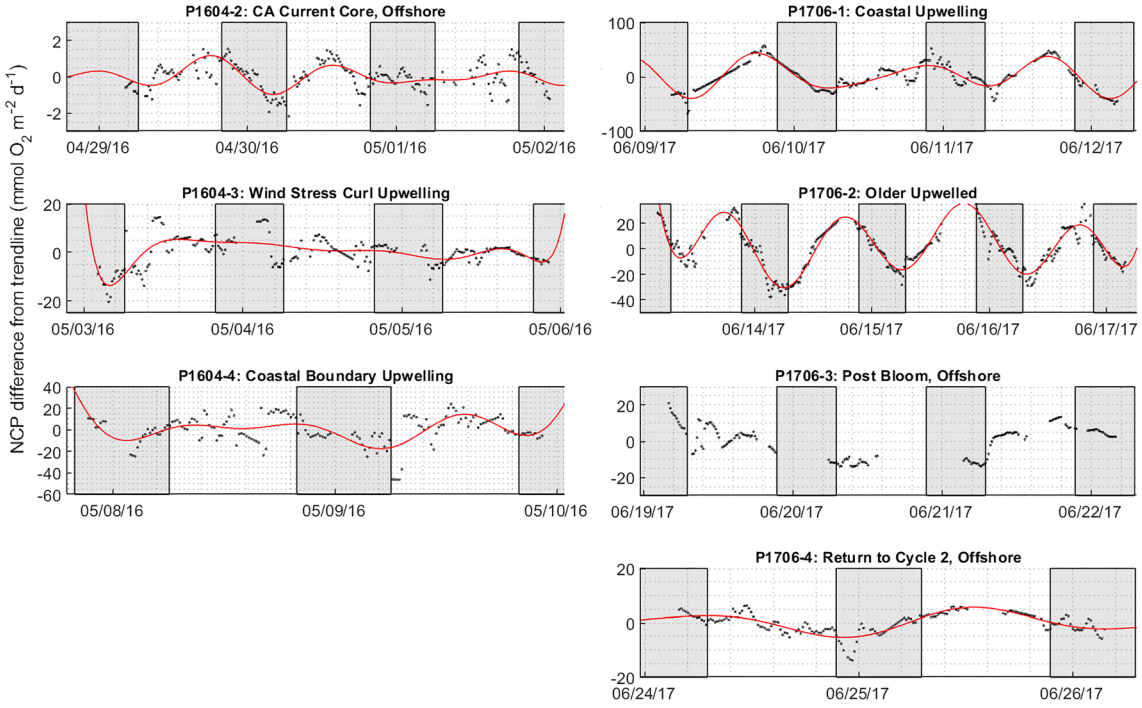


**Figure 5.** $NCP_{prior}$ measured for each Lagrangian cycle and detrended using the linear fits previously obtained (black). The curves corresponding to the Fourier series functions chosen to fit the diel pattern in the NCP data are shown in red. Shaded sections of background indicate nighttime periods.

**Table 3**
*Calculated Mean Diel Range of Diel Cycles in $\Delta O_2/Ar$ and $NCP_{prior}$ Observed During Each Cycle Alongside Mean Volumetric and Integrated Chl-a*

| | Δ $O_2$/Ar range (%) | NCP range (mmol $O_2$ $m^{-2}$ $day^{-1}$) | Chl-*a* (μg $L^{-1}$) | MLD-integrated Chl-*a* (mg $m^{-2}$) |
|---|---|---|---|---|
| P1604-2 | 0.3 | 3 | 0.1 (0.0) | 10 |
| P1604-3 | 3.9 | 26 | 1.1 (0.2) | 17 |
| P1604-4 | 11.4 | 40 | 4.1 (0.8) | 50 |
| P1706-1 | 15.4 | 100 | 9.3 (2.7) | 160 |
| P1706-2 | 4.3 | 67 | 3.1 (1.0) | 76 |
| P1706-3 | 1.4 | 24 | 0.6 (0.5) | 11 |
| P1706-4 | 2.1 | 13 | 0.2 (0.1) | 3 |

and entrainment fluxes appeared to generally increase in both median magnitude and range of values with closer proximity to shore (Table 2).

## 4. Discussion

### 4.1. Differences in Short-Term Nonsteady State and Exponentially Weighted Calculations of NCP

The large difference in median cycle NCP when comparing $NCP_{prior}$ (calculated using an exponential wind speed history weighting) to real time $NCP_{RT}$ is primarily driven by the magnitude of the trend in $\Delta O_2/Ar$ over the length of observations. While changes in measured MLD would affect the $NCP_{RT}$ calculation, the overall offset between $NCP_{RT}$ and $NCP_{prior}$ appears generally dominated by the slope produced by the rate of change in $\Delta O_2/Ar$ over the 2–4 day period. A multiday decrease in $\Delta O_2/Ar$ over time results in a negative offset in which $NCP_{prior}$ rates are significantly greater than $NCP_{RT}$ values, and vice versa. Consequently, $NCP_{prior}$ agrees well with $NCP_{RT}$ when the rate of change in $\Delta O_2/Ar$ is small, as for P1604-2 (Table 2).

Prior studies observing nonsteady state changes in $\Delta O_2/Ar$ over time have attributed part of the rate-of-change term to changes in the biological community, as evidenced by patterns in Chl-*a* over the observational period (Hamme et al., 2012). Based on supporting Advanced Laser Fluorometry measurements from our 2017 cruise (available from the CCE-LTER website), however, we do not observe any multiday increases or decreases in Chl-*a* that might explain the observed nonsteady state trends in biological oxygen saturation anomaly. Intriguingly, we do observe a correspondence between the magnitude of the diel signal changes in $\Delta O_2/Ar$ and diel behavior in Chl-*a* across our cycles (Figure S2), qualitatively supporting the relationship between diel optical particulate organic carbon measurements, reflecting organic biomass, and $^{14}C$ primary production rates established in a study in the North Pacific Subtropical Gyre (White et al., 2017).

It is important to note that $NCP_{prior}$ and $NCP_{RT}$ are not expected to be directly comparable as the integration time for each metric is distinct as previously mentioned. While $NCP_{prior}$ purports to integrate over the residence time of dissolved $O_2$ in the surface mixed layer (several days to weeks), $NCP_{RT}$ is intended to reflect the rate of production over the period of observed measurements only.

We acknowledge that our Lagrangian time series observations were of relatively short duration, subjecting our estimate of the slope term in surface layer $O_2/Ar$ saturation anomaly to some uncertainty. In particular, P1706-4 was occupied for a period of just two days compared to the 3- to 4-day study length employed at other sites. Notably, this cycle, intended as an extension of P1706-2 several days later, differs from P1706-2 considerably in terms of the implied rates of change in $\Delta O_2/Ar$ observed during the two respective cycles (Figure 6). This observation indeed suggests that short deployments (2–3 days) can produce differing rates of change in mixed-layer biological oxygen saturation anomaly compared to calculations using longer-term (weeklong or greater) measurements. Such longer timescales are generally more characteristic of the residence time of biological oxygen in the surface ocean. At the same time, however, the residence time of biological oxygen in the surface layer in this region with respect to the biology is short, as evidenced by rapid changes in oxygen concentrations.

A number of experimental limitations to the Lagrangian design of this study also warrant mention. The possibility does exist that the drogued experimental array drifted relative to the water mass. First, the array is fitted with a surface float, which is subject to surface currents and winds, imparting some influence on the array's trajectory. Second, the array was fitted with racks and bottles for other experiments at several depths, including depths deeper than 15 m. The hydrodynamic drag resulting from the surface float and these bottle experiments is another source of potential divergence between the original water mass and the drogued array.

We also do reemphasize that the California Current system in many ways represents a worst-case environment for the quantification of NCP from EIMS and/or MIMS-based $O_2/Ar$ measurements. Upwelling waters from depth in this region are often highly undersaturated in $O_2/Ar$ and likely violate the assumption of

negligible vertical fluxes frequently. Under certain local conditions, ongoing equilibration between the undersaturated surface mixed layer and the atmosphere may result in apparent $O_2$/Ar undersaturation even while mixed-layer production rates are high and positive. Alternatively, elevated productivity in the surface mixed layer might contribute to $O_2$/Ar supersaturation despite the presence of a strong influence from vertical fluxes of low $O_2$/Ar waters, leading investigators to take productivity rates at face value when they in fact represent underestimates. Multiday trends in $O_2$/Ar can thus be driven by a combination of biology as well as the physics of air-sea gas exchange. Finally, community metabolic rates along this highly productive coast might be of a sufficiently dramatic magnitude to unbalance air-sea exchange from net production/respiration even in the absence of vertical fluxes. Investigators have long cautioned against deploying the $O_2$/Ar method in environments characterized by such factors (Castro-Morales et al., 2013; Haskell & Fleming, 2018; Reuer et al., 2007), and indeed, exponentially weighted $NCP_{prior}$ appears to line up much more closely with $NCP_{RT}$ at greater distance offshore, an environment more typical of settings where the $O_2$/Ar technique has been employed to date.

As a result of these factors, we overall assess $NCP_{RT}$ to be of limited utility in upwelling regions as a means to estimate NCP over short timescales from $O_2$/Ar measurements. Whereas the $d(\Delta O_2/Ar)/dt$ term in $NCP_{RT}$ purportedly corrects for lag between air-sea gas exchange of biological oxygen and real rates of biological oxygen production, it can be impacted by changes in wind speeds as well as shifts in surface ocean biology that occurred prior to the deployment period. Given the significant weight of the $d(\Delta O_2/Ar)/dt$ term as previously noted, such effects introduce considerable uncertainty into $NCP_{RT}$. Furthermore, accurately correcting for vertical fluxes from depth would require not only estimating or measuring such fluxes but correcting for changes in those fluxes over the measurement period. Consequently, $NCP_{RT\_Vflux}$ (see section 2) does not satisfactorily reflect productivity on short timescales but at best can measure the total production or consumption of biological oxygen in the surface mixed layer as a combination of physical and biological processes.

### 4.2. Influence of Diel Patterns in $O_2$/Ar Upon Measured $NCP_{prior}$

Our observation of strong diel signals within Lagrangian observations of the $O_2$/Ar saturation anomaly reinforce earlier findings (Ferron et al., 2015; Hamme et al., 2012; Tortell et al., 2014) that diel effects can be significant across diverse environments, a consequence of the inherently strong influence of the most recent time period upon the recorded $O_2$/Ar signal. Consequently, the time of day can matter considerably when conducting non-Lagrangian measurements, affecting measured values by a factor of 2 or more. We demonstrate that the amplitude of the diel signal increases consistently along a cross-shore gradient in our study region during the growing season, with the effect exhibiting an increased magnitude for a higher productivity regime.

Using our measurements as an example, this phenomenon means that was a vessel hypothetically conducting point measurements of NCP to arrive on-station close to the coast at 3 a.m. as opposed to 3 p.m. local time, the difference in measured NCP calculated from the $\Delta O_2/Ar$ signal might be as large as 20–50 mmol $O_2$ $m^{-2}$ $day^{-1}$: an effect approaching 50% of the median NCP measured at inshore stations. Ultimately, if considering only the effect of biology under constant, nonzero wind speed, this diel factor would bias NCP measurements low if conducted close to dawn and high if taken close to dusk. However, the magnitude of the bias scales proportionally to the total metabolic rate of the surface ocean community, and thus, the absolute effect of diel variations in $O_2$/Ar is low in less productive settings. Nevertheless, due to the lower overall $NCP_{prior}$ rates, diel effects remain a large source of variability in terms of relative proportions.

A consistent trend between both volumetric and MLD-integrated Chl-*a* measurements and diel $O_2$/Ar signal amplitude was observed in both years of our study (Table 3). Consequently, volumetric or depth-integrated Chl-*a* alone may potentially serve as the basis for a field indicator of potential diel variability in biological oxygen saturation anomaly. In this study, we observe that median cycle Chl-*a* concentrations above 1 μg $L^{-1}$ correspond to diel variability in $\Delta O_2/Ar$ on the order of 3% in amplitude or more, suggesting that diel effects are of potential concern for most "productive" ecosystems. However, more Lagrangian observations will likely be required to develop a robust metric that might be used to gauge the risk of significant diel behavior in $O_2$/Ar.

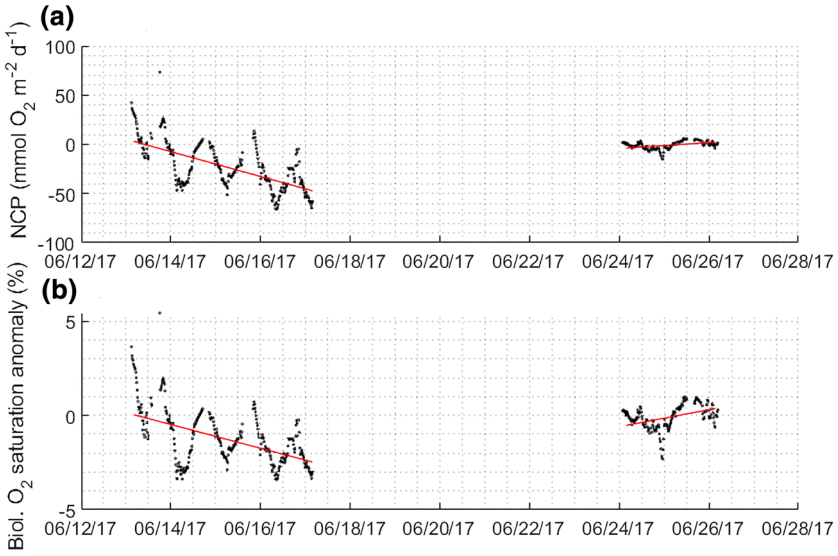


**Figure 6.** Time series of (a) $NCP_{prior}$ and (b) $\Delta O_2/Ar$ saturation anomaly for Cycles 2017 #2 and #4. Red line segments illustrate best fit linear regression lines and trends for each multiday series of observations.

Additionally, we point out that a number of other factors not captured by the surface Chl-*a* inventory may also be responsible for driving diel signals. For instance, it is possible that diel variations in respiration due to heterotrophic activity, potentially due to zooplankton vertical migration or other factors, may also explain a component of the diel $O_2/Ar$ signal, confounding efforts to assess the diel signal amplitude in relation to Chl-*a* alone. Additionally, the magnitude of diel behavior in $O_2/Ar$ is also determined by the extent of gas exchange between the atmosphere and surface ocean, where more vigorous air-sea equilibration may act to dampen the diel cycle. Finally, the influence of other factors like photosynthetically active radiation, light attenuation, and tidal effects may also impact diel variability by influencing the biological community.

Unfortunately, it remains difficult to say how investigators can correct for this diel effect while conducting Eulerian measurements. When deploying underway $O_2/Ar$ measurements at sites of particular interest, a best practice might be to occupy the station for a period extending through a 12-hr period in order to capture the daily range and median of the $O_2/Ar$ signal. However, in practice such an approach may not be possible due to time and logistical constraints. Ultimately, our results reemphasize that such diel effects can be considerable and ought to be factored in when interpreting non-Lagrangian measurements of NCP determined using both discrete and underway $\Delta O_2/Ar$-based approaches.

### 4.3. Influence of Vertical Fluxes of $O_2/Ar$ Upon Apparent $NCP_{prior}$

Overall, we assess the impact of vertical fluxes of $O_2/Ar$ to be a dominant and large influence. The largest vertical flux term overall by a considerable margin comprised the effect of vertical advection, which we calculated to potentially produce fluxes several-fold to a full order of magnitude larger than uncorrected $NCP_{prior}$ rates (Table 2). This finding parallels the conclusions of Haskell and Fleming (2018), who calculated vertical transport fluxes of 50–124 mmol $O_2$ $m^{-2}$ $day^{-1}$ off the California coast in spring 2013 and 2014 that left uncorrected NCP estimates just 15–16% of corrected NCP rates. The dominant impact of vertical fluxes is also supported by $N_2O$-calculated mixing corrections for $O_2/Ar$ NCP measurements off British Columbia that yielded vertical flux contributions of 150–200 mmol $O_2$ $m^{-2}$ $day^{-1}$ in coastal shelf waters in spring and summer that significantly elevated corrected NCP rates by several-fold relative to uncorrected NCP estimates (Izett et al., 2018).

Our vertical flux estimates, however, are considerably larger than estimated vertical contributions from these studies. This may be primarily driven by our strong modeled vertical velocities near the base of the mixed layer in this region, with average velocities during each cycle of 3.8–9.7 m $day^{-1}$. Such vertical velocities are nevertheless within expectations for this region (17–20 m $day^{-1}$, and substantially larger during upwelling events) (Huyer, 1983; Münchow, 2000) and are well within the range of upwelling rates

observed in dynamic ocean regions at the submesoscale (Lévy et al., 2012). In contrast, (Haskell & Fleming, 2018) estimated lower vertical velocities of no more than 4.2 m $day^{-1}$ at the San Pedro Ocean Time-series using the $^{7}$Be tracer approach.

Uncertainty in these vertical advective flux estimates has the potential to produce overestimates of advective fluxes of $O_2$/Ar between the surface layer and subsurface. Modeled vertical velocities may not be consistently reliable for estimating advection, particularly when leveraged on such short time scales. Advection thus represents a considerable factor to correct for but is itself difficult to confidently constrain without direct measurements.

Consequently, we would not consider $NCP_{RT\_Vflux}$ estimates (see section 2) made using $F_{adv}$ calculated in this study to be reliable metrics of vertically corrected productivity. For instance, mean $F_{adv}$ is strongly positive during P1604-4, P1706-1, and P1706-2 due to strong local upwelling of undersaturated waters. Taking such fluxes at face value would produce implausibly high corrected NCP rates (>700 mmol $O_2$ $m^{-2}$ $day^{-1}$). Phytoplankton biomass during those cycles was insufficiently high to produce such rates, with mean *Chl-a* of 3.1 to 9.3 mg $m^{-3}$. In comparison, $^{14}$C primary production measurements during spring and summer blooms in Chesapeake Bay yielded rates of <300 mmol $O_2$ $m^{-2}$ $day^{-1}$ (assuming a photosynthetic quotient of 1.4) despite Chl-*a* measurements as high as 25–27 mg $m^{-3}$ (Adolf et al., 2006). Long-term primary productivity data sets from the California Current region show annual peaks in photic-zone production rates of no more than 150 mmol $O_2$ $m^{-2}$ $day^{-1}$ (Mantyla et al., 2008). Given the high sensitivity of our calculation to the strength and sign of the vertical velocities used, our method for estimating the advective flux term is thus subject to substantial error. Nevertheless, the considerable magnitude of potential vertical advective fluxes reemphasizes the importance of considering vertical advection in this region.

Contributions from nonadvective vertical fluxes of $O_2$ are also nonnegligible, with entrainment fluxes and vertical eddy diffusion also producing estimated fluxes of up to 96 and 22 mmol $O_2$ $m^{-2}$ $day^{-1}$ during some cycle measurements, respectively. Therefore, our assessment also reinforces the need to account for these vertical terms in both Eulerian and Lagrangian surveys employing underway $\Delta O_2$/Ar measurements, as well as discrete $\Delta O_2$/Ar sampling.

When considering the impact of vertical eddy diffusion, entrainment, and advection upon Eulerian $NCP_{prior}$ measurements, however, these fluxes should ideally be evaluated over the residence time of the $O_2$/Ar signal, and we also suggest that time weighting based on the weighted gas transfer velocity approach of Reuer et al. (2007) might be employed to more accurately constrain these terms. Due to our lack of reliable means to estimate subsurface $O_2$ gradients, eddy diffusivities, vertical velocities, and MLD changes prior to our arrival onsite, however, we were unable to evaluate $F_v$, $F_e$, and $F_{adv}$ over a longer, more appropriate timescale. Furthermore, our Lagrangian study approach here allowed us to neglect horizontal advective fluxes and focus only on vertical terms. When using an Eulerian sampling approach, the inclusion of horizontal advection terms might lead to significant impacts. We further note that Eulerian surveys of $NCP_{prior}$ in fact represent point measurements of exponentially weighted NCP over the past Lagrangian path of the water parcel, meaning that an ideal accounting of vertical fluxes would hypothetically track the influence of such terms in space and time along the same path. One potentially fruitful approach for future incorporation of vertical advection into NCP calculations would be to use mean upwelling velocities derived from simulated Lagrangian particles, rather than velocities from the Eulerian model. If such Lagrangian particles were released backward in time from the measurement location, their dispersion in space would give an estimate of the multiple historical upwelling trajectories that brought water to the sampling location. Such a Lagrangian model is, however, beyond the scope of this study.

At a minimum, vertical profiles of oxygen from frequent CTD casts can be employed as demonstrated here to assess the impact of these factors. Preferably, discrete or high-frequency vertical sampling of the $O_2$/Ar ratio with depth can greatly improve the accuracy and confidence of such calculations. At the same time, the recently developed $N_2O$ method (Cassar & Manizza, 2014) also shows promise (Izett et al., 2018) as an approach for correcting the influence of vertical fluxes by simultaneously quantifying multiple sources of vertical mixing. We suggest that this method simplifies the complications detailed above regarding attempts to model vertical physical $O_2$/Ar fluxes and the difficulty of back-calculating their magnitude along the Lagrangian path traveled by sampled water masses. However, this method is also limited by assumptions,

including negligible $N_2O$ production in the mixed layer and minimal horizontal heterogeneity. Alternatively, direct measurements of vertical mixing using approaches such as the $^7$Be method (Kadko & Johns, 2011) could directly quantify the strength of mixing, although this technique possesses a different residence time relative to $O_2$, and incorporating the method may present logistical challenges for cruise planners.

We do note that our calculations of vertical fluxes utilize measurements of $O_2$ and $O_2$ gradients rather than $O_2$/Ar, and therefore involve the assumption that changes in $O_2$ with depth are mirrored by the $O_2$/Ar signal. Typically, fairly small gradients in Ar saturation are expected with depth within the first few hundred meters from the surface (Hamme et al., 2019; Hamme & Severinghaus, 2007), with deviations of under 2% saturation anomaly from surface values. Nevertheless, our use of $O_2$ concentrations for vertical flux calculations represents a potential source of error if Ar saturation was in fact significantly variable over the first couple hundred meters below the surface layer. Finally, our vertical flux calculations likely represent overestimates of the overall vertical $O_2$/Ar transport, as they do not account for horizontal divergence at the surface layer.

To summarize, vertical advection is generally the more important vertical $O_2$/Ar flux relative to eddy diffusion and mixed-layer entrainment, with advection a particularly difficult-to-constrain source of uncertainty. The contribution of vertical fluxes to the mixed-layer $O_2$/Ar budget, however, is dependent on local conditions, particularly on upwelling rates and the strength of the vertical gradient in biological oxygen. Overall, the effect of vertical fluxes of $O_2$/Ar also appears to be of major importance to consider, capable of introducing very large uncertainties into calculations of $NCP_{prior}$ in this region.

## 5. Conclusions

Ultimately, our study further highlights the importance of considering the potential impact of vertical fluxes, diel variation, and the specific timescales of interest when assessing surface layer productivity using in situ $\Delta O_2$/Ar measurements, particularly within a highly productive, dynamic region such as the CCE. Taking advantage of our Lagrangian study design as well as model output data, we are able to contrast exponentially weighted $NCP_{prior}$ rates calculated using traditional assumptions with shorter-term NCP estimates calculated without reliance on a steady-state condition and also assess the potential influence of vertical fluxes. We conclude that the nonsteady state rate of change term represents a considerable influence upon attempts to estimate short-term NCP rates in this region. At the same time, we observe the calculated and potential influence of vertical fluxes of $O_2$/Ar from entrainment, vertical eddy diffusion, and particularly vertical advection to be significant, contributing substantially to the real mixed-layer $O_2$/Ar budget.

We reiterate that our study region and results represent conditions that have long been held to be poorly suited to deployment of the in situ $O_2$/Ar method. While assumptions of negligible vertical fluxes may be valid for given regions and seasons, such factors should nevertheless be assessed in any field deployment to ensure that their potential impact is truly small. Techniques such as the $N_2O$ approach for quantifying the influence of vertical fluxes upon $O_2$/Ar (Cassar & Manizza, 2014) may be well suited to help correct EIMS or MIMS measurements of NCP conducted in environments presenting similar challenges to the California Current system (Izett et al., 2018).

Similarly, when performing non-Lagrangian measurements in regions of high diel metabolic activity, we find that adequate consideration of the impact of time of day upon measured values is also important. We observed diel cycles in $\Delta O_2$/Ar of up to 17% in range at some locations, adding a considerable source of variability to the median cycle $\Delta O_2$/Ar signal on hourly time scales. Lastly, our study highlights conditions under which diel and multiday nonsteady state factors exert relatively low influence over calculated NCP rates. Less productive ecosystems more characteristic of the open ocean, with Chl-*a* concentrations below 1 μg $L^{-1}$ tend to exhibit both lower diel variability as well as considerably smaller absolute offsets between NCP estimated using steady-state versus nonsteady state assumptions.

To alleviate the influence of such diel impacts on future studies, we suggest that when monitoring throughout the course of the solar day at a field location is not possible, investigators should endeavor to capture $O_2$/Ar measurements that cover a 12-hr period fully capturing the local daily solar maximum. Another logical next step would be the identification of a clear predictor for diel nonsteady state conditions, using metrics such as Chl-*a*, MLD, wind speed, or other parameters, to flag biased conditions while in the field.

While vertical flux effects as well as diel patterns in $\Delta O_2/Ar$ can be considerable in the field, particularly within highly productive and physically dynamic settings, investigators possess means to evaluate the impact of such factors upon in situ productivity rate estimates. Our findings within a challenging study environment reemphasize the importance of critically evaluating basic assumptions inherent to the $O_2/Ar$ method and stress the utility of careful planning and study design when conducting $O_2/Ar$ measurements under nonideal conditions.

**Acknowledgments**
This research was made possible by a RAPID NSF OCE-1614359 and federal funding provided to the California Current Ecosystem (CCE) LTER project, NSF OCE-1637632. H. S. acknowledges the support by National Research Foundation of Korea (NRF) grant funded by the Korea Government (MSIT) (NRF-2019R1C1C1003663) and Yonsei University Research Fund of 2018-22-0053. We are sincerely grateful to the captain, crew, and marine technicians of the *R/V Sikuliaq* and the *R/V Roger Revelle* for their assistance prior to and during our 2016 and 2017 expeditions. We are additionally thankful for helpful suggestions and input from Susan Lozier, Laifang Li, Sijia Zou, and Kimberly Drouin, as well as reviewer feedback from Roberta Hamme and one anonymous reviewer. We also thank Susan Becker, Melissa Miller, and Megan Roadman for their assistance processing and analyzing collected Winker samples. We are additionally grateful to Ralf Goericke for his help processing vessel cruise data and to Chief Scientist Mark Ohman and the rest of the CCE LTER team. Lastly, we thank the staff of Scripps Institution of Oceanography for their cruise logistical and organizational support. The authors declare no conflict of interest. Data reported and presented in this study can be accessed under the P1706 and P1604 categories at the CCE-LTER Datazoo online database (https://oceaninformatics.ucsd.edu/datazoo/catalogs/ccelter/datasets).

## References

Adolf, J. E., Yeager, C. L., Miller, W. D., Mallonee, M. E., & Harding, L. W. (2006). Environmental forcing of phytoplankton floral composition, biomass, and primary productivity in Chesapeake Bay, USA. *Estuarine, Coastal and Shelf Science*, *67*(1), 108–122. https://doi.org/10.1016/j.ecss.2005.11.030

Bender, M. L., Kinter, S., Cassar, N., & Wanninkhof, R. (2011). Evaluating gas transfer velocity parameterizations using upper ocean radon distributions. *Journal of Geophysical Research: Oceans*, *116*(C2). https://doi.org/10.1029/2009JC005805

Berger, W. H., & Wefer, G. (1990). Export production: Seasonality and intermittency, and paleoceanographic implications. *Palaeogeography, Palaeoclimatology, Palaeoecology*, *89*(3), 245–254. https://doi.org/10.1016/0031-0182(90)90065-F

Cassar, N., Barnett, B., Bender, M., Kaiser, J., Hamme, R., & Tilbrook, B. (2009). Continuous high-frequency dissolved $O_2/Ar$ measurements by equilibrator inlet mass spectrometry. *Analytical Chemistry*, *81*(5), 1855–1864. https://doi.org/10.1021/ac802300u

Cassar, N., DiFiore, P. J., Barnett, B. A., Bender, M. L., Bowie, A. R., Tilbrook, B., et al. (2011). The influence of iron and light on net community production in the Subantarctic and Polar Frontal Zones. *Biogeosciences*, *8*(2), 227–237. https://doi.org/10.5194/bg-8-227-2011

Cassar, N., & Manizza, M. (2014). Correcting oceanic $O_2$/Ar-net community production estimates for vertical mixing using $N_2O$ observations. *Geophysical Research Letters*, *41*(24), 8961–8970. https://doi.org/10.1002/2014GL062040

Castro-Morales, K., Cassar, N., Shoosmith, D. R., & Kaiser, J. (2013). Biological production in the Bellingshausen Sea from oxygen-to-argon ratios and oxygen triple isotopes. *Biogeosciences*, *10*(4), 2273–2291. https://doi.org/10.5194/bg-10-2273-2013

Chavez, F. P., Messié, M., & Pennington, J. T. (2010). Marine primary production in relation to climate variability and change. *Annual Review of Marine Science*, *3*(1), 227–260. https://doi.org/10.1146/annurev.marine.010908.163917

Chelton, D. B., Univ. of Calif., San Diego, La Jolla. (1982). Large-scale response of the California Current to forcing by the wind stress curl CalCOFI Rep. 23, 130–148 Calif.

Craig, H., & Hayward, T. (1987). Oxygen supersaturation in the ocean: Biological versus physical contributions. *Science*, *235*(4785), 199. Retrieved from–202. http://science.sciencemag.org/content/235/4785/199.abstract, https://doi.org/10.1126/science.235.4785.199

Dong, S., Sprintall, J., Gille, S. T., & Talley, L. (2008). Southern Ocean mixed-layer depth from Argo float profiles. *Journal of Geophysical Research*, *113*, C06013. https://doi.org/10.1029/2006JC004051

Doyle, J. D., Jiang, Q. F., Chao, Y., & Farrara, J. (2009). High-resolution real-time modeling of the marine atmospheric boundary layer in support of the AOSN-II field campaign. *Deep-Sea Research Part Ii-Topical Studies in Oceanography*, *56*(3–5), 87–99. https://doi.org/10.1016/j.dsr2.2008.08.009

Ducklow, H. W., & Doney, S. C. (2013). What is the metabolic state of the oligotrophic ocean? A debate. *Annual Review of Marine Science*, *5*(1), 525–533. https://doi.org/10.1146/annurev-marine-121211-172331

Dugdale, R. C., & Goering, J. J. (1967). Uptake of new and regenerated forms of nitrogen in primary productivity. *Limnology and Oceanography*, *12*(2), 196. &. Retrieved from <Go to ISI>://WOS:A19679423500002

Emerson, S., Stump, C., & Nicholson, D. (2008). Net biological oxygen production in the ocean: Remote in situ measurements of $O_2$ and $N_2$ in surface waters. *Global Biogeochemical Cycles*, *22*(3). https://doi.org/10.1029/2007gb003095

Eveleth, R., Cassar, N., Sherrell, R. M., Ducklow, H., Meredith, M. P., Venables, H. J., et al. (2017). Ice melt influence on summertime net community production along the Western Antarctic Peninsula. *Deep Sea Research Part II: Topical Studies in Oceanography*, *139*, 89–102. https://doi.org/10.1016/j.dsr2.2016.07.016

Ferron, S., Wilson, S. T., Martinez-Garcia, S., Quay, P. D., & Karl, D. M. (2015). Metabolic balance in the mixed layer of the oligotrophic North Pacific Ocean from diel changes in $O_2/Ar$ saturation ratios. *Geophysical Research Letters*, *42*(9), 3421–3430. https://doi.org/10.1002/2015gl063555

Field, C. B., Behrenfeld, M. J., Randerson, J. T., & Falkowski, P. (1998). Primary production of the biosphere: Integrating terrestrial and oceanic components. *Science*, *281*(5374), 237–240. https://doi.org/10.1126/science.281.5374.237

Fofonoff, N. P., & Millard Jr, R. C. (1983). Algorithms for the computation of fundamental properties of seawater. Paris, France, UNESCO, 53pp. (UNESCO Technical Papers in Marine Sciences; 44)

Garcia, H. E., & Gordon, L. I. (1992). Oxygen solubility in seawater: Better fitting equations. *Limnology and Oceanography*, *37*(6), 1307–1312. Retrieved from <go to ISI>://WOS:A1992KR91400015

Garcia, H. E., & Gordon, L. I. (1993). Erratum: Oxygen solubility in seawater: Better fitting equations. *Limnology and Oceanography*, *38*(3), 656.

Hamme, R. C., Cassar, N., Lance, V. P., Vaillancourt, R. D., Bender, M. L., Strutton, P. G., et al. (2012). Dissolved $O_2/Ar$ and other methods reveal rapid changes in productivity during a Lagrangian experiment in the Southern Ocean. *Journal of Geophysical Research-Oceans*, *117*, C00F12. https://doi.org/10.1029/2011JC007046

Hamme, R. C., Nicholson, D. P., Jenkins, W. J., & Emerson, S. R. (2019). Using noble gases to assess the ocean's carbon pumps. *Annual Review of Marine Science*, *11*(1), 75–103. https://doi.org/10.1146/annurev-marine-121916-063604

Hamme, R. C., & Severinghaus, J. P. (2007). Trace gas disequilibria during deep-water formation. *Deep-Sea Research Part I-Oceanographic Research Papers*, *54*(6), 939–950. https://doi.org/10.1016/j.dsr.2007.03.008

Haskell Ii, W. Z., Prokopenko, M. G., Stanley, R. H. R., & Knapp, A. N. (2016). Estimates of vertical turbulent mixing used to determine a vertical gradient in net and gross oxygen production in the oligotrophic South Pacific gyre. *Geophysical Research Letters*, *43*(14), 7590–7599. https://doi.org/10.1002/2016GL069523

Haskell, W. Z., & Fleming, J. C. (2018). Concurrent estimates of carbon export reveal physical biases in ΔO2/Ar-based net community production estimates in the Southern California Bight. *Journal of Marine Systems*, *183*, 23–31. https://doi.org/10.1016/j.jmarsys.2018.03.008

Hodur, R. M. (1997). The Naval Research Laboratory's coupled ocean/atmosphere mesoscale prediction system (COAMPS). *Monthly Weather Review*, *125*(7), 1414–1430. https://doi.org/10.1175/1520-0493(1997)125<1414:tnrlsc>2.0.co;2

Hutchins, D. A., DiTullio, G. R., Zhang, Y., & Bruland, K. W. (1998). An iron limitation mosaic in the California upwelling regime. *Limnology and Oceanography*, *43*(6), 1037–1054. https://doi.org/10.4319/lo.1998.43.6.1037

Huyer, A. (1983). Coastal upwelling in the California current system. *Progress in Oceanography*, *12*(3), 259–284. https://doi.org/10.1016/0079-6611(83)90010-1

Izett, R. W., Manning, C. C., Hamme, R. C., & Tortell, P. D. (2018). Refined estimates of net community production in the subarctic Northeast Pacific derived from $O_2$/Ar measurements with $N_2O$-based corrections for vertical mixing. *Global Biogeochemical Cycles*, *32*(3), 326–350. https://doi.org/10.1002/2017gb005792

Jonsson, B. F., Doney, S. C., Dunne, J., & Bender, M. (2013). Evaluation of the Southern Ocean $O_2$/Ar-based NCP estimates in a model framework. *Journal of Geophysical Research: Biogeosciences*, *118*, 385–399. https://doi.org/10.1002/jgrg.20032

Juranek, L. W., Hamme, R. C., Kaiser, J., Wanninkhof, R., & Quay, P. D. (2010). Evidence of $O_2$ consumption in underway seawater lines: Implications for air-sea $O_2$ and $CO_2$ fluxes. *Geophysical Research Letters*, *37*, L01601. https://doi.org/10.1029/2009gl040423

Kadko, D., & Johns, W. (2011). Inferring upwelling rates in the equatorial Atlantic using $^7$Be measurements in the upper ocean. *Deep Sea Research Part I: Oceanographic Research Papers*, *58*(6), 647–657. https://doi.org/10.1016/j.dsr.2011.03.004

Kaiser, J., Reuer, M. K., Barnett, B., & Bender, M. L. (2005). Marine productivity estimates from continuous $O_2$/Ar ratio measurements by membrane inlet mass spectrometry. *Geophysical Research Letters*, *32*, L19605. https://doi.org/10.1029/2005gl023459

Kelly, T. B. (2019). An open source pipeline for $O_2$ Ar flux analysis.

King, A. L., & Barbeau, K. (2007). Evidence for phytoplankton iron limitation in the southern California Current System. *Marine Ecology Progress Series*, *342*, 91–103. https://doi.org/10.3354/meps342091

Kranz, S. A., Wang, S., Kelly, T. B., Stukel, M. R., Goericke, R., Landry, M. R., & Cassar, N. (2020). Lagrangian studies of marine production: A multimethod assessment of productivity relationships in the California Current Ecosystem upwelling region. *Journal of Geophysical Research: Oceans*, *125*, e2019JC015984. https://doi.org/10.1029/2019JC015984

Landry, M. R., Ohman, M. D., Goericke, R., Stukel, M. R., Barbeau, K. A., Bundy, R., & Kahru, M. (2012). Pelagic community responses to a deep-water front in the California Current Ecosystem: Overview of the A-Front Study. *Journal of Plankton Research*, *34*(9), 739–748. https://doi.org/10.1093/plankt/fbs025

Landry, M. R., Ohman, M. D., Goericke, R., Stukel, M. R., & Tsyrklevich, K. (2009). Lagrangian studies of phytoplankton growth and grazing relationships in a coastal upwelling ecosystem off Southern California. *Progress in Oceanography*, *83*(1–4), 208–216. https://doi.org/10.1016/j.pocean.2009.07.026

Lévy, M., Ferrari, R., Franks, P. J. S., Martin, A. P., & Rivière, P. (2012). Bringing physics to life at the submesoscale. *Geophysical Research Letters*, *39*, L14602. https://doi.org/10.1029/2012GL052756

Li, Z. C., & Cassar, N. (2017). A mechanistic model of an upper bound on oceanic carbon export as a function of mixed layer depth and temperature. *Biogeosciences*, *14*(22), 5015–5027. https://doi.org/10.5194/bg-14-5015-2017

Lynn, R. J., & Simpson, J. J. (1987). The California Current System: The seasonal variability of its physical characteristics. *Journal of Geophysical Research*, *92*(C12), 12947-12966. https://doi.org/10.1029/JC092iC12p12947

Mantyla, A. W., Bograd, S. J., & Venrick, E. L. (2008). Patterns and controls of chlorophyll-a and primary productivity cycles in the Southern California Bight. *Journal of Marine Systems*, *73*(1), 48–60. https://doi.org/10.1016/j.jmarsys.2007.08.001

Miller, A. J., Song, H., & Subramanian, A. C. (2015). The physical oceanographic environment during the CCE-LTER years: Changes in climate and concepts. *Deep-Sea Research Part II—Topical Studies in Oceanography*, *112*, 6–17. https://doi.org/10.1016/j.dsr2.2014.01.003

Moore, A. M., Arango, H. G., Broquet, G., Powell, B. S., Weaver, A. T., & Zavala-Garay, J. (2011). The Regional Ocean Modeling System (ROMS) 4-dimensional variational data assimilation systems Part I—System overview and formulation. *Progress in Oceanography*, *91*(1), 34–49. https://doi.org/10.1016/j.pocean.2011.05.004

Morrow, R. M., Ohman, M. D., Goericke, R., Kelly, T. B., Stephens, B. M., & Stukel, M. R. (2018). CCE V: Primary production, mesozooplankton grazing, and the biological pump in the California Current Ecosystem: Variability and response to El Nino. *Deep-Sea Research Part I-Oceanographic Research Papers*, *140*, 52–62. https://doi.org/10.1016/j.dsr.2018.07.012

Münchow, A. (2000). Wind stress curl forcing of the Coastal Ocean near Point Conception, California. *Journal of Physical Oceanography*, *30*(6), 1265–1280. https://doi.org/10.1175/1520-0485(2000)030<1265:WSCFOT>2.0.CO;2

Munro, D. R., Quay, P. D., Juranek, L. W., & Goericke, R. (2013). Biological production rates off the Southern California coast estimated from triple $O_2$ isotopes and $O_2$: Ar gas ratios. *Limnology and Oceanography*, *58*(4), 1312–1328. https://doi.org/10.4319/lo.2013.58.4.1312

Nickels, C. F., & Ohman, M. D. (2018). CCEIII: Persistent functional relationships between copepod egg production rates and food concentration through anomalously warm conditions in the California Current Ecosystem. *Deep-Sea Research Part I—Oceanographic Research Papers*, *140*, 26–35. https://doi.org/10.1016/j.dsr.2018.07.001

Niiler, P. P., Sybrandy, A. S., Bi, K. N., Poulain, P. M., & Bitterman, D. (1995). Measurements of the water-following capability of holey-sock and TRISTAR drifters. *Deep-Sea Research Part I-Oceanographic Research Papers, 42*(11-12), 1951-&. https://doi.org/10.1016/0967-0637(95)00076-3

Ohman, M. D., Barbeau, K., Franks, P. J. S., Goericke, R., Landry, M. R., & Miller, A. J. (2013). Ecological transitions in a coastal upwelling ecosystem. *Oceanography*, *26*(3), 210–219. https://doi.org/10.5670/oceanog.2013.65

Ohman, M. D., Powell, J. R., Picheral, M., & Jensen, D. W. (2012). Mesozooplankton and particulate matter responses to a deep-water frontal system in the southern California Current System. *Journal of Plankton Research*, *34*(9), 815–827. https://doi.org/10.1093/plankt/fbs028

Reuer, M. K., Barnett, B. A., Bender, M. L., Falkowski, P. G., & Hendricks, M. B. (2007). New estimates of Southern Ocean biological production rates from $O_2$/Ar ratios and the triple isotope composition of $O_2$. *Deep-Sea Research Part I—Oceanographic Research Papers*, *54*(6), 951–974. https://doi.org/10.1016/j.dsr.2007.02.007

Rykaczewski, R. R., & Checkley, D. M. (2008). Influence of ocean winds on the pelagic ecosystem in upwelling regions. *Proceedings of the National Academy of Sciences of the United States of America*, *105*(6), 1965–1970. https://doi.org/10.1073/pnas.0711777105

Song, H., Miller, A. J., McClatchie, S., Weber, E. D., Nieto, K. M., & Checkley, D. M. (2012). Application of a data-assimilation model to variability of Pacific sardine spawning and survivor habitats with ENSO in the California Current System. *Journal of Geophysical Research*, *117*, C03009. https://doi.org/10.1029/2011JC007302

Stanley, R. H., Kirkpatrick, J. B., Cassar, N., Barnett, B. A., & Bender, M. L. (2010). Net community production and gross primary production rates in the western equatorial Pacific. *Global Biogeochemical Cycles 24*, GB4001. https://doi.org/10.1029/2009GB003651

Strub, P. T., & James, C. (2000). Altimeter-derived variability of surface velocities in the California Current System: 2. Seasonal circulation and eddy statistics. *Deep-Sea Research Part Ii-Topical Studies in Oceanography*, *47*(5–6), 831–870. https://doi.org/10.1016/s0967-0645(99)00129-0

Stukel, M. R., Ohman, M. D., Benitez-Nelson, C. R., & Landry, M. R. (2013). Contributions of mesozooplankton to vertical carbon export in a coastal upwelling system. *Marine Ecology Progress Series*, *491*, 47−+. https://doi.org/10.3354/meps10453

Teeter, L., Hamme, R. C., Ianson, D., & Bianucci, L. (2018). Accurate estimation of net community production from $O_2$/Ar measurements. *Global Biogeochemical Cycles*, *32*(8), 1163–1181. https://doi.org/10.1029/2017GB005874

Thomas, B. R., Kent, E. C., & Swail, V. R. (2005). Methods to homogenize wind speeds from ships and buoys. *International Journal of Climatology*, *25*(7), 979–995. https://doi.org/10.1002/joc.1176

Tortell, P. D. (2005). Dissolved gas measurements in oceanic waters made by membrane inlet mass spectrometry. *Limnology and Oceanography: Methods*, *3*(1), 24–37. https://doi.org/10.4319/lom.2005.3.24

Tortell, P. D., Asher, E. C., Ducklow, H. W., Goldman, J. A. L., Dacey, J. W. H., Grzymski, J. J., et al. (2014). Metabolic balance of coastal Antarctic waters revealed by autonomous $pCO_2$ and Delta $O_2$/Ar measurements. *Geophysical Research Letters*, *41*(19), 6803–6810. https://doi.org/10.1002/2014gl061266

Ulfsbo, A., Cassar, N., Korhonen, M., van Heuven, S., Hoppema, M., Kattner, G., & Anderson, L. G. (2014). Late summernet community production in the central Arctic Ocean using multiple approaches. *Global Biogeochemical Cycles*, *28*(10), 1129–1148. https://doi.org/10.1002/2014gb004833

Wang, S., Lin, Y., Gifford, S., Eveleth, R., & Cassar, N. (2018). Linking patterns of net community production and marine microbial community structure in the western North Atlantic. *The ISME Journal*. *12*(11), 2582–2595. https://doi.org/10.1038/s41396-018-0163-4

Wanninkhof, R. (2014). Relationship between wind speed and gas exchange over the ocean revisited. *Limnology and Oceanography: Methods*, *12*(6), 351–362. https://doi.org/10.4319/lom.2014.12.351

White, A. E., Barone, B., Letelier, R. M., & Karl, D. M. (2017). Productivity diagnosed from the diel cycle of particulate carbon in the North Pacific Subtropical Gyre. *Geophysical Research Letters*, *44*(8), 3752–3760. https://doi.org/10.1002/2016gl071607

Williams, P. J. L., Von Bodungen, B., Bathman, U., Berger, W. H., Eppley, R. W., Feldman, G. C., et al. (1989). Group report: Export productivity from the photic zone. In W. H. Berger, V. Smetacek, & G. Wefer (Eds.), *Productivity of the Ocean: Present and Past*, (pp. 99–115). Hoboken, N.J: John Wiley and Sons.